Supplemental Tables

Table S1: Antibody information

Antigen	Antibody	Dilution
Active β-CATENIN	Millipore 05-665	1:400
BRACHYURY	R&D Systems AF-2085	1:300
E-CADHERIN	Cell Signalling 3195	1:200
E-CADHERIN	Abcam 40772	1:400
FRZD7	R&D Systems MAB1981	1:200
LEF1	Cell Signalling 2230	1:200
LRP6	R&D Systems 1505	1:100
N-CADHERIN	BioLegend 350802	1:200
SMAD2	BD bioscience 610842	1:100
SOX17	R&D Systems AF-1924	1:200
SOX2	Cell Signalling 3579	1:200

Table S2: RT-QPCR Primer designs

Gene Symbol	Forward primer	Reverse Primer
AXIN2	ctccccaccttgaatgaaga	tggctggtgcaaagacatag
BRACHYURY	catgcaggtgagttgtcagaa	gctgtgacaggtacccaacc
CER1	gccatgaagtacattgggaga	cacagccttcgtgggttatag
DKK1	ccttggatgggtattccaga	cctgaggcacagtctgatga
DKK3	agagcctgatggagccttg	ggcttgcacacatacaccag
LEF1	agatcaccccacctcttgg	atgagggatgccagttgtgt
LEFTY1	ctgcacaccctggacctt	atcccctgcaggtcaatgta
LEFTY2	cctggacctcagggactatg	atcccctgcaggtcaatgta
SFRP1	gctggagcacgagaccat	tggcagttcttgttgagca
SFRP2	gctagcagcgaccacctc	tttttgcaggcttcacatacc

Table S3: sgRNA designs

Gene Symbol	Forward primer	Reverse Primer
CER1	caccgcttcctcatggttgcctgt	aaacacaggcaaccatgaggaagc
DKK1	caccgtctggtacttattcccgcc	aaacggcgggaataagtaccagac
DKK3	caccgtctcattgtgatagctggg	aaaccccagctatcacaatgagac
E-CAD	caccgcagcagcagcagcgccgag	aaacctcggcgctgctgctgctgc
LEFTY1	caccggtcatccccacccacgtga	aaactcacgtgggtggggatgacc
SFRP1	caccggagcacgagaccatggcgg	aaacccgccatggtctcgtgctcc
SFRP2	caccggtggtcgctgctagcgagg	aaaccctcgctagcagcgaccacc

Table S4: Knockout lines

Target	Separate clones
RUES2:DKK1$^{-/-}$	3
RUES2-GLR:DKK1$^{-/-}$	2
RUES2:DKK3$^{-/-}$	2
RUES2:E-CAD$^{-/-}$	2
RUES2:CER1$^{-/-}$	1
RUES2:LEFTY1$^{-/-}$	1
RUES2:SFRP1$^{-/-}$	1
RUES2:SFRP2$^{-/-}$	1
RUES2:SFRP1$^{-/-}$SFRP2$^{-/-}$	1
RUES2:LEFTY1$^{-/-}$CER1$^{-/-}$	1

Supplemental Figures

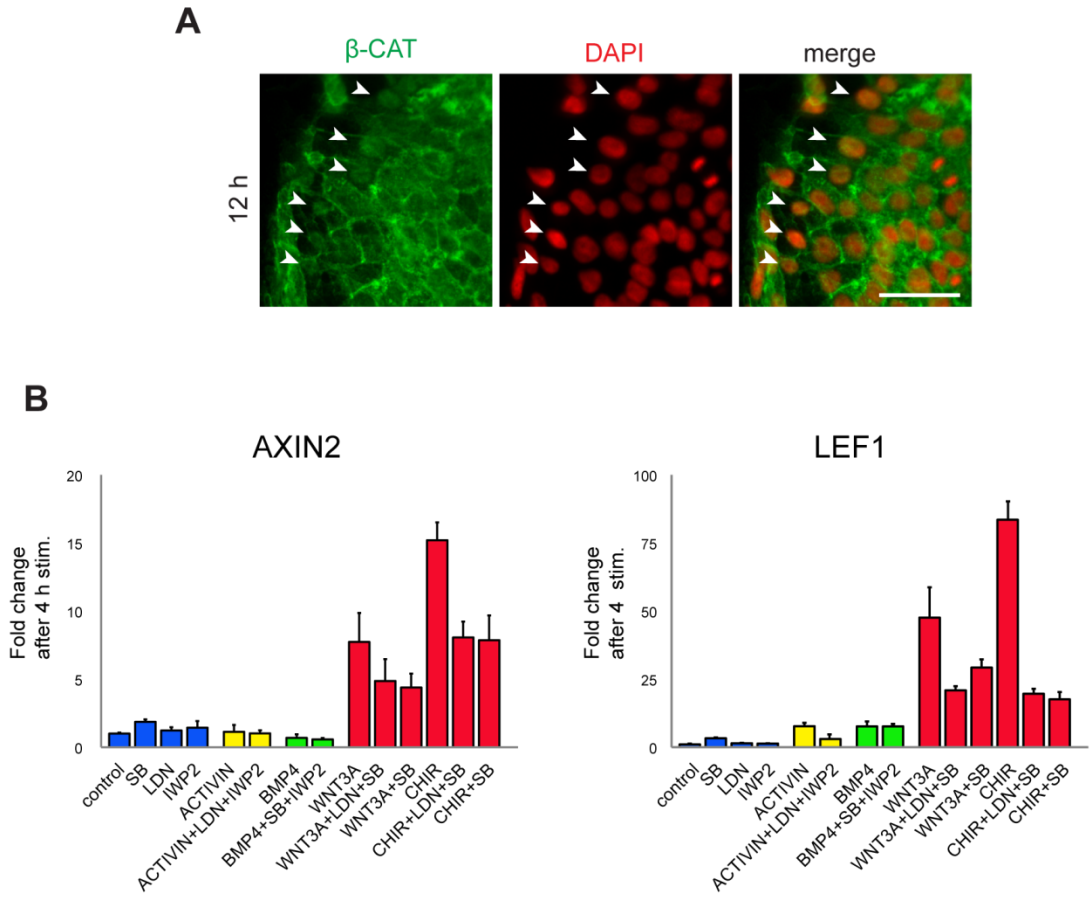

Figure S1 | WNT3A response markers

(A) Inset of an abnormally low density micropattern colony stimulated with WNT3A and fixed and stained at 12h for active β-CATENIN. Even at this low density (seeded with $6x10^5$ cells, stimulated 2 hours after seeding) an increase in β-CAT in the nucleus is only visible in loosely connected cells on the colony edge (arrows). Nuclear β-CATENIN in cells away from the periphery or at higher density (including standard low density conditions) is not easily observed, largely due to signal from membrane-bound or cytoplasmic regions. Scale bar, 50µm.

(B) qPCR of AXIN2 and LEF1 as a function of inputs arrayed on x-axis. The results show that the LEF1 and AXIN2 response is dominated by WNT3A, though synergism with the NODAL pathway is significant as well, as can be seen by comparing WNT3A or CHIR with WNT3A+SB or CHIR+SB. Thus LEF1 and AXIN2 can be used as proxies for early WNT3A response. Also note that LEF1 gives a greater positive signal than AXIN2, reaching 84-fold induction compared with 15 fold induction for CHIR condition.

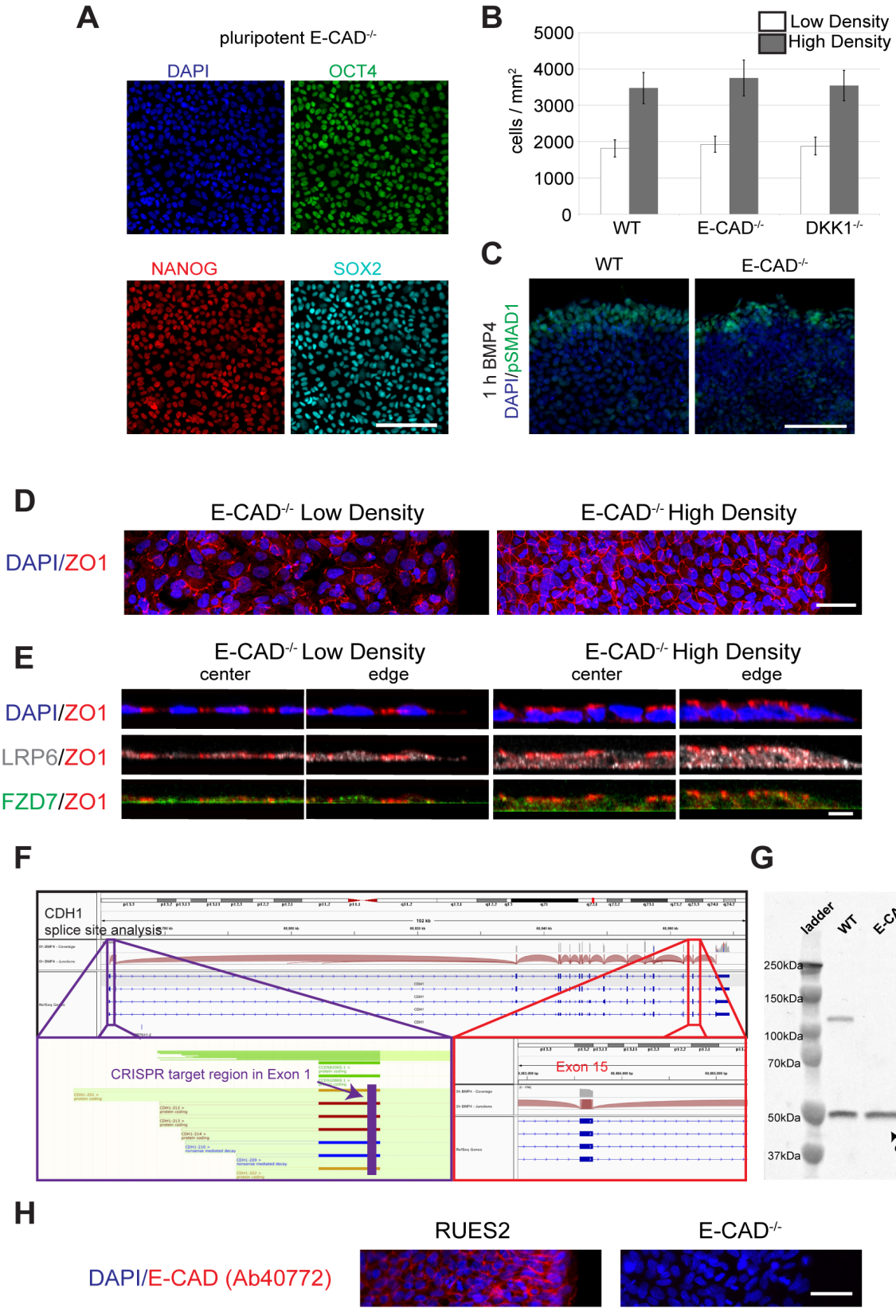

Figure S2 | Epithelial integrity is preserved in E-CAD$^{-/-}$ cells.

(A) E-CAD$^{-/-}$ cells maintain pluripotency markers even with continual passaging (i.e. >20 passages). Images are of unpatterned, standard hESC culture colonies. Scale bar, 100µm.

(B) E-CAD$^{-/-}$ cell seeding efficiency and growth is similar to wild type and DKK1-/- cell lines.

(C) Test of epithelial integrity and BMP4 response. Edge of high density wild type and E-CAD$^{-/-}$ micropatterns stimulated with BMP4 and fixed and stained for pSmad1 after 1h. As in the wild type, pSMAD1 expression is restricted to the periphery in E-CAD$^{-/-}$ colonies. Scale bar, 100µm.

(D) Maximum intensity projection of ZO1 and DAPI in low density and high density E-CAD$^{-/-}$ micropatterns immediately prior to stimulation. The network of tight junctions is the same as in the wild type (Figure 1C). Scale bar, 50µm.

(E) Cross-sections showing the apical-basal position of WNT receptors relative to DAPI and ZO1. Result is the same as for wild type micropaterns (Figure 1D). Scale bar, 10µm.

(F) Top: sashimi plot in Integrative Genomics Viewer of E-CAD region from previously published RNA-seq data set[1] showing exon splicing pattern observed in RUES2 cells in pluripotency conditions. Bottom left: zoom of Exon 1 region in Ensembl viewer showing the four different E-CAD isoforms and the sgRNA CRISPR targeting site used. Bottom right: zoom of Exon 15 region that the Cell Signalling 3195 E-CAD antibody targets. As one can see from the plot, there is no isoform that skips this exon.

(G) Western blot of pluripotent wild type and E-CAD$^{-/-}$ cells for E-CAD and α-tubulin. One can see that while E-CAD and α-tubulin are detected in the wild type cells, only α-tubulin is visible in the knockout cell line.

(H) Staining of pluripotent wild type and E-CAD$^{-/-}$ cells with Abcam anti-E-CADHERIN ab40772 antibody that targets amino acids 600-700. One can see that while E-CAD is detected in the wild type cells, no E-CAD is visible in the knockout cell line. Scale bar, 50µm.

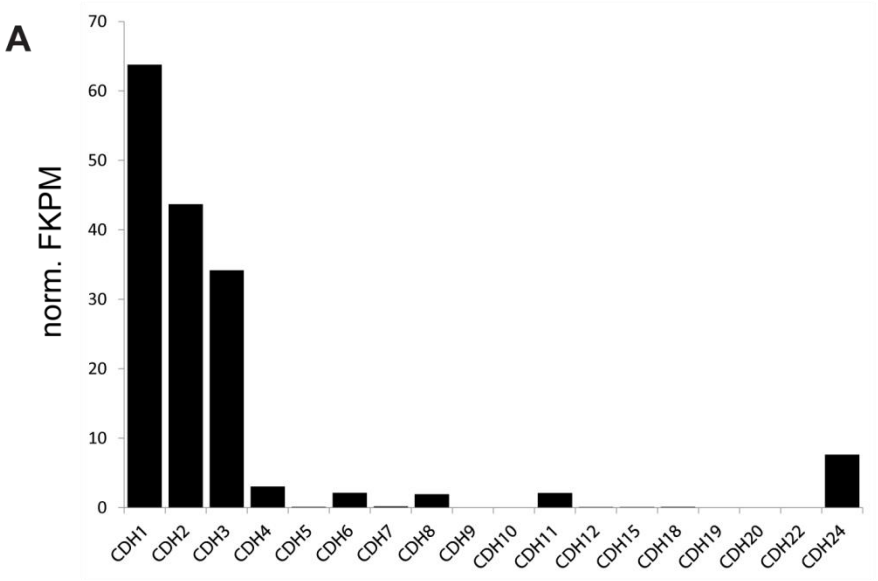

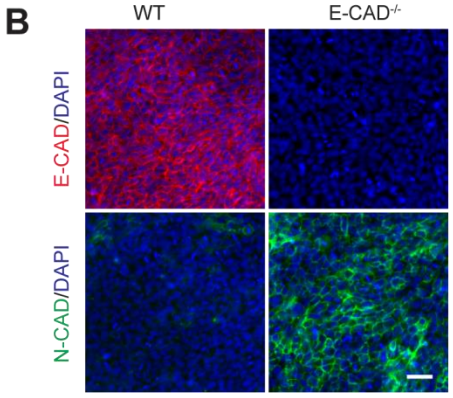

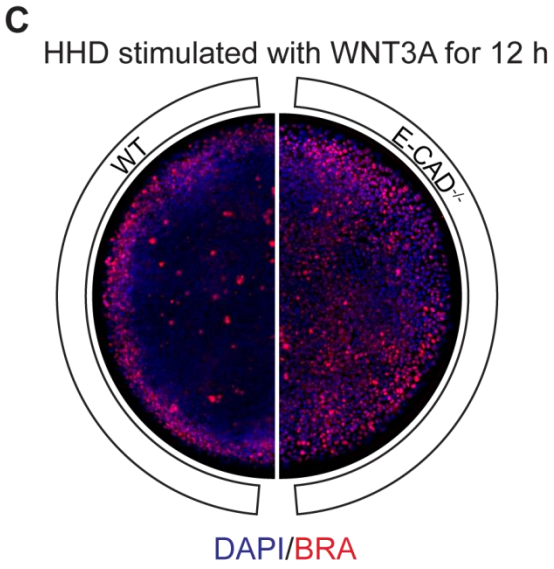

Figure S3 | A change in the protein expression profile of N-CADHERIN occurs in the E-CAD$^{-/-}$ cell line.

(A) RNA-seq profiling for all classic cadherins in pluripotent hESCs. Since the E-CAD (CDH1) knockout is lethal in mouse at the post-compaction stage, we were somewhat surprised at the lack of an E-CAD$^{-/-}$ pluripotent phenotype (Supplemental Figure 2). However both N-CADHERIN and P-CADHERIN (CDH2,CDH3) are substantially expressed at the mRNA level in hESCs in pluripotency.

(B) Stain for N-CAD and E-CAD in wild type and E-CAD$^{-/-}$ in unpatterned pluripotent colonies. Antibody stain for E-CAD confirms that gene is knocked out in E-CAD$^{-/-}$ cells. More interestingly, while N-CAD is barely visible in wild-type cells, N-CAD is highly expressed and membrane localized in E-CAD$^{-/-}$ cells. Thus there is a reservoir of N-CAD message in hESC that is only expressed in the absence of E-CAD, which may be a consequence of the same pathway that up regulates N-CAD during EMT when the transcription of E-CAD is abrogated by SNAIL. Interestingly, other research has shown that the artificial replacement E-CAD protein by N-CAD protein in the mouse intestine after gastrulation showed that N-CAD could fulfill the structural role of E-CAD, but the replacement lead to an up-regulation of WNT signalling that is also consistent with our findings[2]. Scale bar, 50µm.

(C) 12h WNT3A response measured by BRA in high high density (HHD) wild type and E-CAD$^{-/-}$ micropatterns. HHD micropatterns are left to grow for an additional 36h beyond that of HD micropatterns before stimulating with WNT3A. One sees that even at this extreme the knockdown of E-CAD allows a WNT3A response into the center of the micropattern.

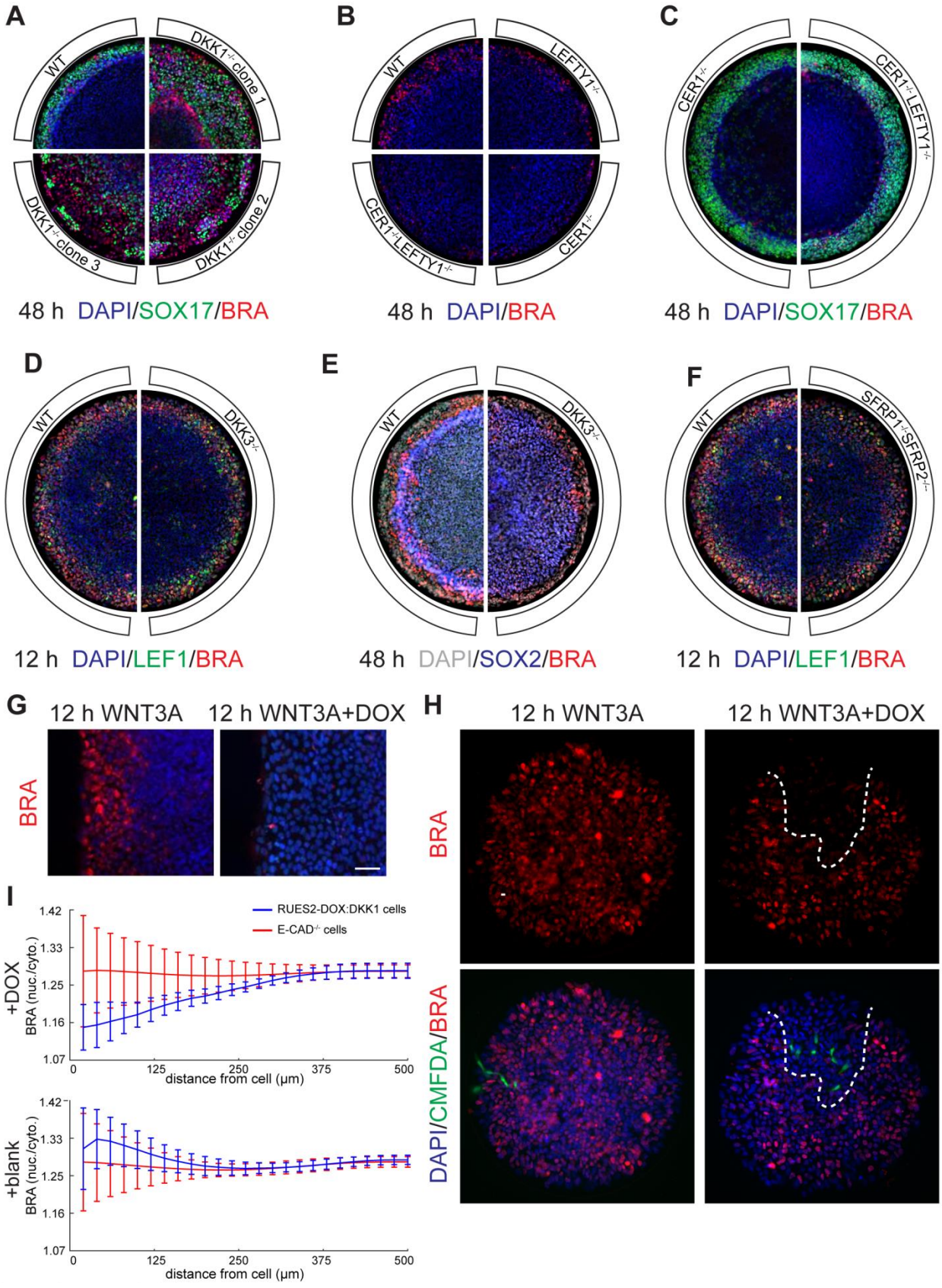

Figure S4 | Other inhibitor CRISPR knockout line and clones

(A) Other DKK1$^{-/-}$ clonal lines with different frameshift mutations also exhibit the same micropattern phenotype when stimulated with WNT3A at high density and fixed and stained after 48 hours.

(B) No discernible difference in SOX17 expression at 48h between CER1$^{-/-}$ and CER1$^{-/-}$LEFTY1$^{-/-}$ micropatterns under WNT3A stimulation.

(C) LEFTY1$^{-/-}$ micropatterns show no discernible difference with wild type micropatterns in number of BRA cells. However, both CER1$^{-/-}$ and CER1$^{-/-}$LEFTY1$^{-/-}$ (with a different CER1 frameshift mutation) show similar phenotype in having fewer BRA cells. Thus CER1$^{-/-}$ and not LEFTY1$^{-/-}$ is the main NODAL inhibitor during WNT induced patterning.

(D) and (E) No discernible difference at 12h or 48h between wild type and DKK3$^{-/-}$ micropatterns under WNT3A stimulation.

(F) No discernible difference at 12h between wild type and SFRP1$^{-/-}$SFRP2$^{-/-}$ micropatterns under WNT3A stimulation.

(G) Edge of a high density 1000µm diameter RUES2-DOX:DKK1-V5 micropattern. Cells were either given DOX or blank media for 12 h and then stimulated with WNT3A for a further 12 h (again with or without DOX continuing the pre-treatment). Cells were then stained for BRA. Scale bar, 50µm.

(H) 500µm diameter E-CAD$^{-/-}$ micropatterns seeded with 1% CMFDA cell tracker marked RUES2-DOX:DKK1-V5 cells (green). Cells were either given DOX or blank media for 12 h immediately after RI removal, and then stimulated with WNT3A for a further 12 h (again with or without DOX continuing the pre-treatment). Micropatterns were then fixed and stained for DAPI and BRA. In the DOX induced micropatterns one can see a BRA exclusion zone around the DKK1 expressing cells (marked roughly with dashed line).

(I) Quantification of (H). 5 DOX-induced and 5 blank stimulated micropatterns were segmented and all cells were first classified as either RUES2-DOX:DKK1-V5 (green) or E-CAD$^{-/-}$ cells. For each cell the nuclear to cytoplasmic ratio of BRA in all neighbouring cells within radius r (x-axis) was calculated and averaged. These averages were then averaged across all cells of their cell type (50 for RUES2-DOX:DKK1-V5, and 5000 for E-CAD$^{-/-}$) and plotted as shown with error bars indicating the standard deviation. One can see that in the DOX induced micropatterns the cells neighbouring the RUES2-DOX:DKK1-V5 cells show lower BRA than the average, and this effect is half-maximal at a distance of ~130µm, showing long-range action. This shielding does not happen when one looks at just neighbours of E-CAD$^{-/-}$cells, or in the blank stimulated micropatterns.

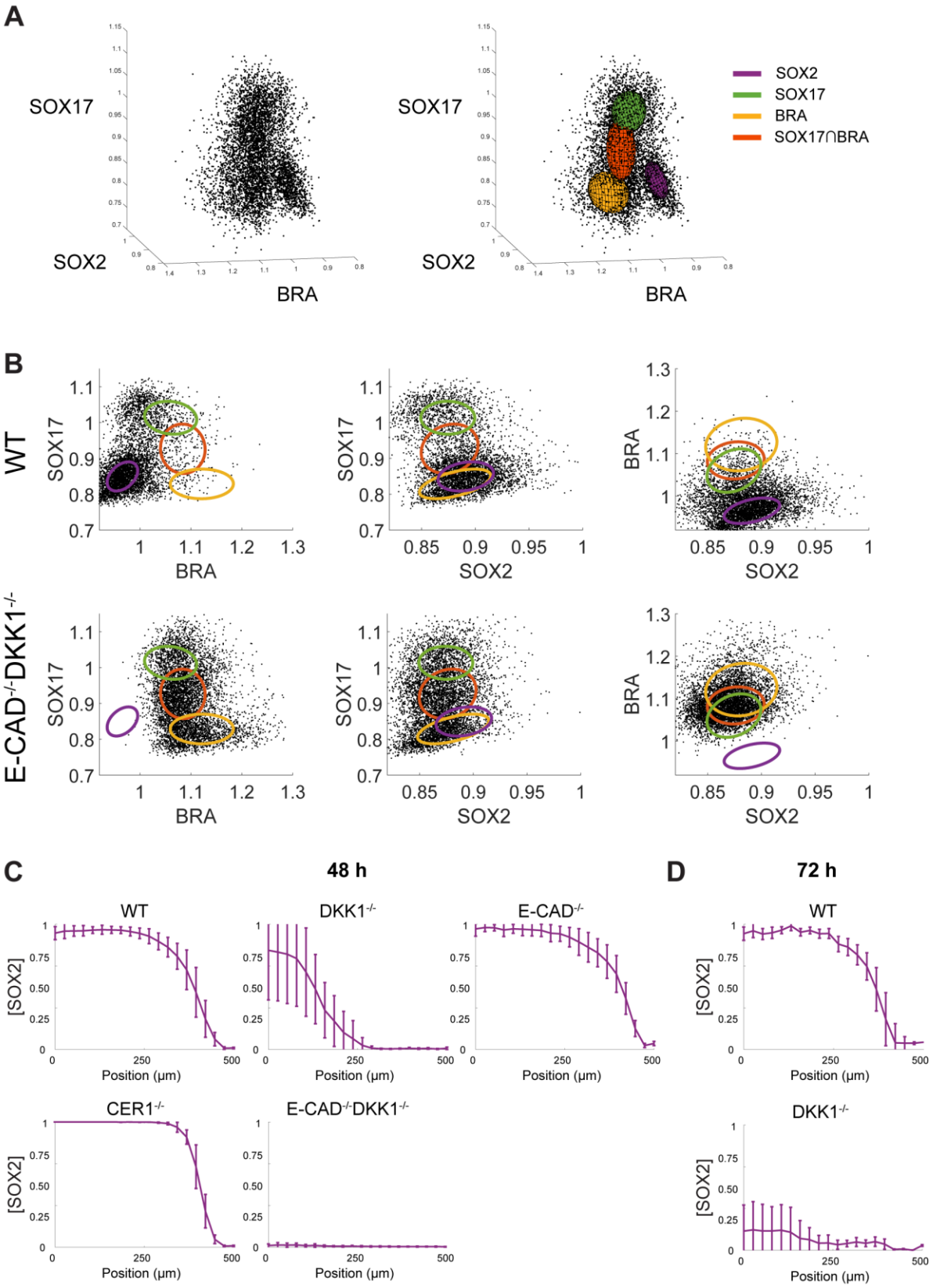

Figure S5 | Fate clustering and classification

(A) 3D scatterplots of combined cells from wild type, DKK1$^{-/-}$, E-CAD$^{-/-}$, E-CAD$^{-/-}$DKK1$^{-/-}$, and CER1$^{-/-}$ 48 h micropatterns data showing clustering into the Gaussian mixture model used for Figure 5D.

(B) Example scatterplots of cells from wild type and E-CAD$^{-/-}$DKK1$^{-/-}$ micropatterns projected into 2D for better visualization of the clustering.

(C) Proportion of cells classified as SOX2+ at 48 h plotted as a function of colony radius. Error bars represent the standard deviation of *n=20* colonies.

(D) Proportion of cells from micropatterns in Figure 6A classified as SOX2+ at 72 h plotted as a function of radius. Error bars represent the standard deviation of *n=20* colonies.

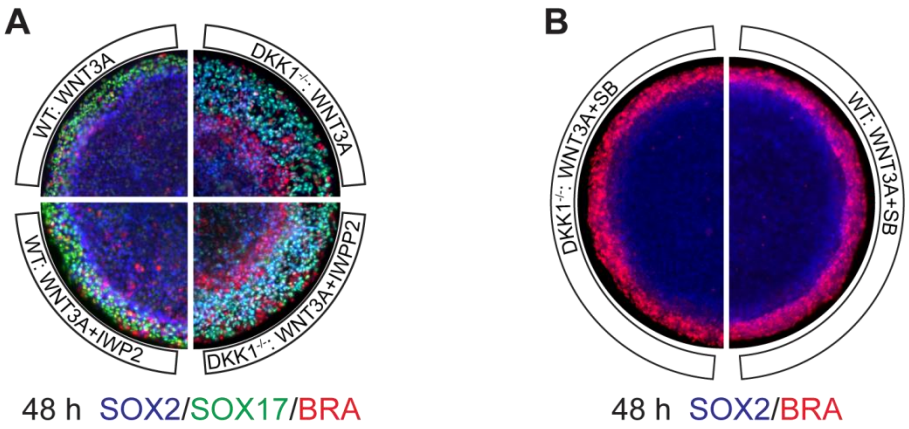

Figure S6 | Endogenous WNT signalling has little effect on patterning

(A) Wild type and DKK1$^{-/-}$ high density micropatterns stimulated with either WNT3A or WNT3A+IWP2 for 48h and stained for BRA, SOX2, and SOX17. No significant differences between wild type IWP2 and non-IWP2 or DKK1$^{-/-}$ IWP2 and non-IWP2 stimulated colonies were observed.

(B) Wild type and DKK1$^{-/-}$ high density micropatterns stimulated with WNT3A+SB for 48h and stained for BRA and SOX2.

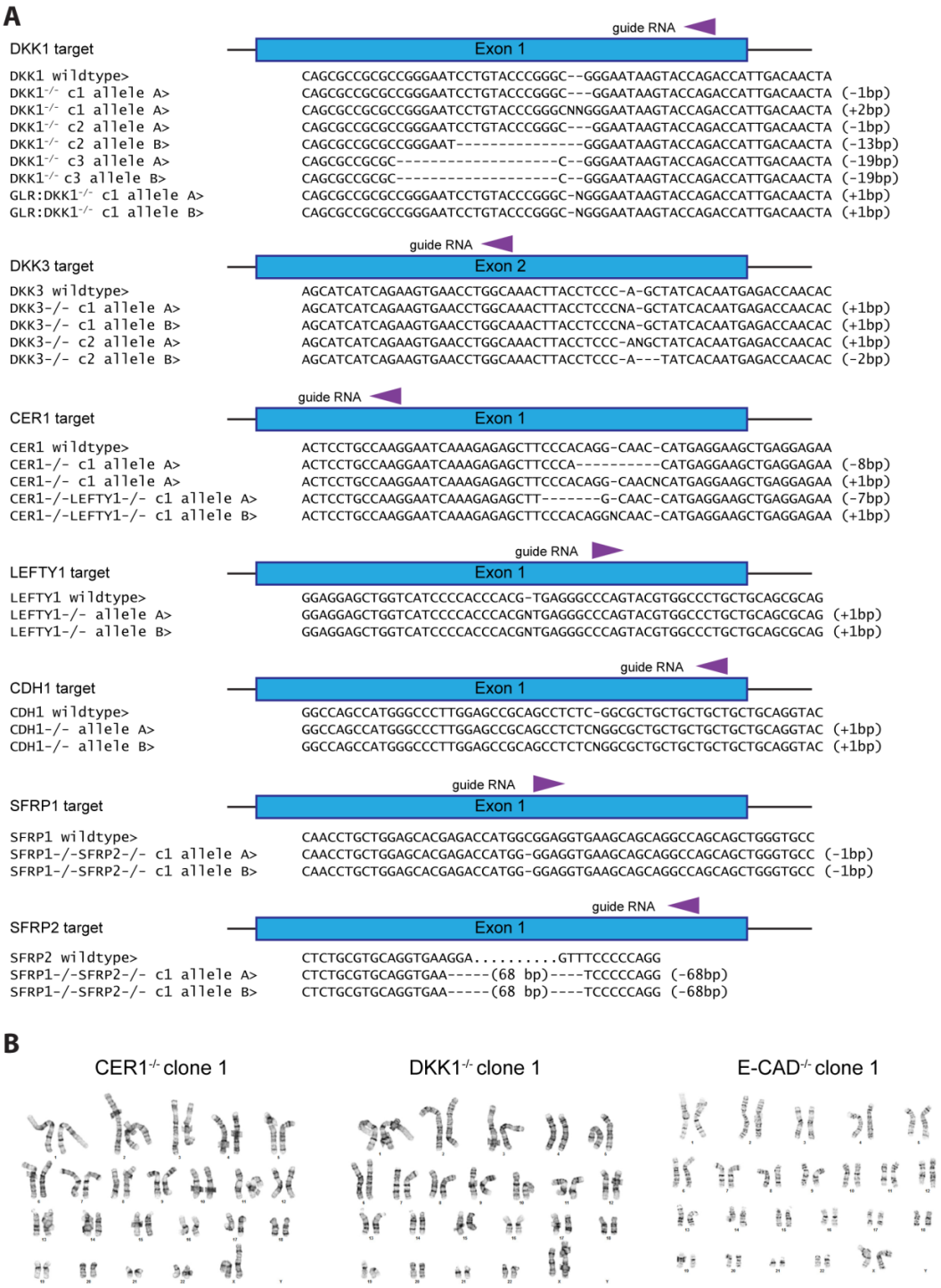

Figure S7 | Confirmation of CRISPR knockouts

(A) Sequences of the mutated alleles in the CRISPR/Cas9 knockout cell lines.

(B) The E-CAD$^{-/-}$ clone 1, DKK1$^{-/-}$ clone 1, and CER1$^{-/-}$ clone 1 cell lines were karyotypically normal.

Supplementary Materials and Methods: Modelling

1 Overview

In this supplement we present a minimal model that fits the micropattern WNT3A phenotype data for each CRISPR knockout cell line. The four key features of this data that the model captures are:

1. The geometric edge bias mediated by E-CAD.
2. The edge restriction of the WNT response by the secreted inhibitor DKK1.
3. The edge-to-interior EMT and WNT response wave, as especially observed in the DKK1$^{-/-}$ line.
4. The bifucation of WNT differentiated cells to mesoderm versus endoderm depending on the relative levels of NODAL signal received.

To capture the first three features we need a model with two spatial diffusion terms: (1) to describe the spreading of DKK1 and its loss from the colony edge, and (2) to describe the implicit cell-cell communication via E-CAD that is responsible for the EMT wave as explained in the main text. As will be shown, this part of the model will give us the WNT signal received by cells at a given radius at a given time and can be used to determine the proportion of differentiated cells at 48hrs after stimulation. As will also be shown, this part of the model consists of 10 parameters, 4 of which can be independently fitted to the E-CAD$^{-/-}$ phenotype, 5 of which can be fitted independently to the DKK1$^{-/-}$ phenotype, and 1 which can be estimated from the E-CAD$^{-/-}$DKK1$^{-/-}$ cell line.

To capture the last feature (the bifurcation of differentiated cells into either mesoderm or endoderm), ideally one would use detailed data of the gene regulatory networks for mesendoderm formation and mesoderm and endoderm bifurcation. However, these are not known to the required level of detail, and so we instead simply use the NODAL signalling level as defined by nuclear SMAD2 to determine fates, with cells with higher nuclear SMAD2 being more likely to be directed to endoderm rather than mesoderm.

2 PDE System

In the first part of the model we need to track three quantities: the WNT response, the level of DKK1, and the level of E-CAD. We let $W(r,t)$ represent the WNT response, we let $I(r,t)$ represent DKK1, and we let $E(r,t)$ represent E-CAD. $W(r,t)$ is the only quantity that we measure experimentally and that we use to fit the model (measured as nuclear LEF1 at 12hrs and at late times, the relative loss of SOX2 i.e., 1-SOX2 after rescaling). Since all of the relevant experiments were conducted on 1000μm diameter disc micropatterns, this 2D geometry is the only geometry we consider in our model as well (though it can be easily generalized to other geometries).

Initial conditions: We assume that $W(r,t)$and $I(r,t)$ are off everywhere and that $E(r,t)$ is uniformly on. For the boundary condition on $W(r,t)$, we take this variable to be cell intrinsic, thus there is no diffusion of $W(r,t)$.

Boundary conditions: For the boundary condition on $I(r,t)$, we assume that it behaves like the BMP secreted inhibitor NOGGIN in the modelling of Etoc et al[1]. Thus DKK1 can freely diffuse over the colony

and is quickly lost to the media on the edge, giving the boundary condition $I(R,t)=0$. Finally, for $E(r,t)$, since the E-CAD state of a cell also depends on its neighbours, we allow for a simple diffusion-like coupling with strength D_E. We do not initially know the scale of this dependence, whether it just immediate neighbours or if the coupling is long range. Thus D_E is one of the key parameters to be fitted, and, as will be shown, it has a direct effect on the speed of the EMT wave. For the boundary condition, we have experimentally that cells on the periphery of the micropatterns have a reduced inhibitory E-CAD effect and are thus more sensitive to WNT3A ligand (see Main Text and especially Figure 2 and Supplemental Figure 2). We incorporate this observation by setting $E(R,t)=0$.

To model the interaction between the WNT response, DKK1, and E-CAD, simple Michaelis–Menten dynamics with activation and inhibition between the three species as shown in Figure 7A suffice. Mechanistically, we justify these interactions as follows: the inhibition of WNT by DKK1 is at the receptor level and is well known[3]; the activation of DKK1 by WNT is at the transcription level and was shown in Figure 4; the inhibition of E-CAD by WNT is also at the transcription level, though it operates more indirectly by WNT first turning on SNAIL and working with FGF[4] (which is always present and constant in our media); and there is extensive literature on the interaction of E-CAD with β-catenin and the effect this has on WNT signalling[5]. For this last interaction, we choose to model it as $E+W\rightarrow E$, i.e. akin to simple enzymatic degradation instead of a more complicated sequestration/release mechanism that might be modelled as $E+W\rightleftharpoons C, C\rightarrow\emptyset$. We make this choice because although there is some evidence for this latter picture[6], much of the dynamic details of how E-CAD affects WNT signalling remain to be worked out. Thus in lieu of a more detailed mechanism, we use simple enzymatic degradation as a reasonable phenomenological approximation of the system, and we find that we achieve a better, more robust fit with it than with the sequestration/release model, even though the latter has more variables.

Since the scales on the three dynamical variables depend on imaging conditions and are thus arbitrary, we can absorb certain constants into their definitions without affecting the generality of the model. We set the maximum rate of synthesis of E-CAD to be equal to ν_E, the rate of natural E-CAD decay, so that in pluripotency the E-CAD level in each cell is 1. Likewise, we set the maximum rate of the WNT response to be equal to its degradation rate ν_W so that the WNT response varies from 0 to 1. We also assume, based on our evidence of direct induction of DKK1 by WNT (Figure 4) that this WNT response rate is a good approximation for the rate of DKK1 synthesis. The coefficient of W in equation (2) can be chosen to equal the degradation rate of W in (1) by adjusting the scale of I so we do not require a DKK1 specific synthesis rate. We do though let DKK1 have its own degradation rate ν_I.

Combining all of the above we obtain:

$$\frac{dW(r,t)}{dt}=\nu_W\frac{\theta_W^n}{\theta_W^n+I^n}-kEW-\nu_W W \qquad (1)$$

$$\frac{dI(r,t)}{dt}=D_I\nabla^2 I+\nu_W W-\nu_I I \qquad (2)$$

$$\frac{dE(r,t)}{dt} = D_E \nabla^2 E + \nu_E \left(\frac{\theta_E^m}{\theta_E^m + W^m} - E \right) \qquad (3)$$

Note that if we are purely interested in exploring the possible dynamics we could simplify this system further, rescaling the time for example so that $t = \tau * t_0$ with $t_0 = 1/\nu_W$. However, as we wish to use this model to fit our data, we need a match of the timescales between model and experiment, and hence we need to fit ν_W. Fortunately, we can get help in estimating its value since in the E-CAD$^{-/-}$DKK1$^{-/-}$ cell line the PDE system reduces to the one parameter equation:

$$\frac{dW(r,t)}{dt} = \nu_W(1 - W) \qquad (4)$$

A fit of the qPCR measured LEF1 response in small, unpatterned colonies of E-CAD$^{-/-}$DKK1$^{-/-}$ cells at various times results in a value of $\nu_W = 0.24/hr$ (Figure S8). The upper and lower 95% confidence bounds are 0.07 and $0.40/hr$. Since this estimate is based on mRNA data and so represents an upper limit, we restrict our search of possible ν_W values to be between 0.07 and $0.24/hr$. We find that the final best fit value is $\nu_W = 0.11/hr$, which means that $W(r,t)$ would reaches its half-maximal value ~6 hours after stimulation if the inhibition of E-CAD and DKK1 are not included.

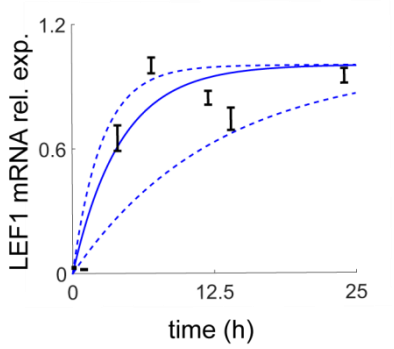

Figure S8: Solid line indicates best fit of LEF1 qPCR timecourse in unpatterned E-CAD$^{-/-}$DKK1$^{-/-}$ cells to Equation 4. Dashed lines indicate 95% confidence interval in the fit. $\nu_W = 0.24\ (0.07, 0.40)$. Error bars represent the standard deviation of three biological replicates.

2.1 Fitting DKK1 and WNT interaction with E-CAD$^{-/-}$ cell line

In the E-CAD$^{-/-}$ cell line the system reduces to just equations (1) and (2) with $E(r,\tau) = 0$. This leaves just 4 parameters to be fitted: n, θ_w, D_I and ν_I. This parameter space is small enough that we can perform a simple exhaustive grid search to find the global optima where the model WNT response curve at 12 and 48hrs matches the data at 12 hours (measured by LEF1) and 48 hours (measured by BRA or SOX17 in Figure 6, which is also equivalent to 1-SOX2) as calculated by a least squares fit. Where possible, this grid search was centered on biologically relevant values for variables, or from previous similar simulations[1].

Figure S9 shows the best fit to the data. The Hill parameter n can adjust the slope of the curve, but the effects of the other parameters are less obvious. To understand these effects we do two things: (1) we

perturb each parameter individually and see the change to the fit, and (2), we let the remaining parameters adapt to the perturbed parameter to see if and how the perturbation can be corrected. Doing this we can see for example that doubling D_I means that more cells on the boundary respond to WNT. Allowing the other parameters to vary while holding the doubled D_I constant, we can also see that decreasing ν_I can counteract this perturbation. This makes sense as increased D_I means more inhibitor is lost and decreasing ν_I counteracts this by making the inhibitor degrade less. The opposite is also true, since halving D_I means fewer cells on the boundary respond to WNT and this effect can be counteracted by increasing ν_I. For the WNT response threshold θ_w, we find that doubling it leads to less inhibitor and more differentiation, and that this can be counteracted by lowering the DKK1 degradation rate. Halving θ_w can conversely be counteracted by increasing ν_I. Taken together, these results imply that there is some redundancy between certain parameters in our model. This is not surprising as although we formulated our model to be minimal in the number of parameters, we also based it directly on the known biology and variables that could be easily perturbed. A more abstract model with a reduced number of variables might give more independent parameter estimates, but it would be harder to explore and relate to the fundamental biology at hand.

Perturbing the E-CAD$^{-/-}$ fit

	D_I (mm^2h^{-1})	ν_I (h^{-1})	θ_W
(1)	0.0024	0.0017	0.3000
(2)	0.0046	0.0017	0.3000
(3)	0.0046	0.0009	0.2073
(4)	0.0012	0.0017	0.3000
(5)	0.0012	0.0034	0.3628
(6)	0.0024	0.0850	0.3000
(7)	0.0022	0.0850	0.1893
(8)	0.0024	0	0.3000
(9)	0.0025	0	0.3045
(10)	0.0024	0.0017	0.5442
(11)	0.0013	0.0017	0.5442
(12)	0.0024	0.0017	0.1361
(13)	0.0050	0.0066	0.1361

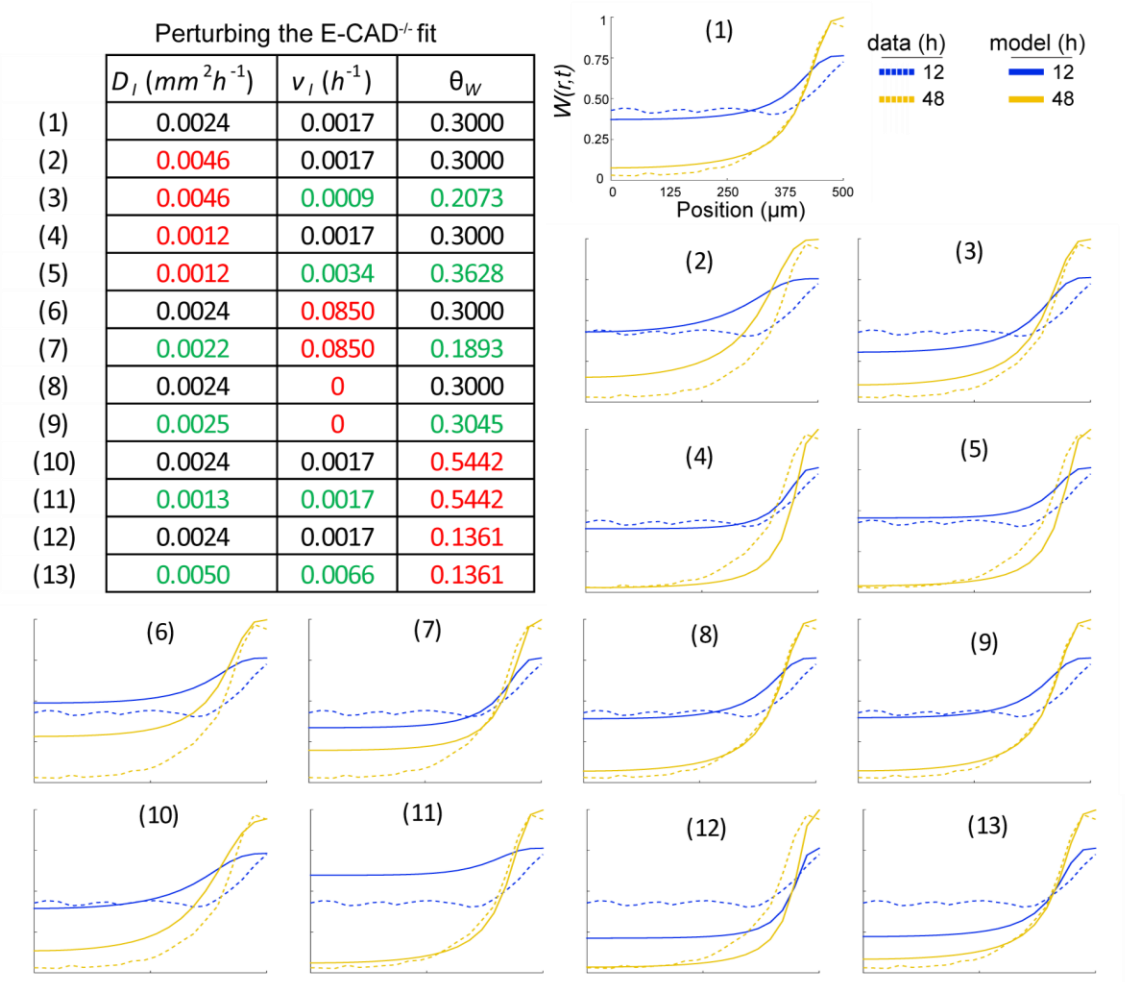

Figure S9: Fit of DKK1 specific parameters with E-CAD $^{-/-}$cell line, and parameter analysis using specific perturbations. Values in black in the table are the best fit parameters, values in red are the parameters specifically perturbed, and values in green are the new best fit parameters based on the perturbed parameter.

2.2 Fitting E-CAD and WNT interaction with DKK1$^{-/-}$ cell line

In the DKK1$^{-/-}$ cell line the system reduces to just equations (1) and (3), with $I(r,\tau)=0$. As can be seen when solving for $W(r,\tau)$ in equilibrium (see Equation 5), this system undergoes a super-critical pitchfork or "cusp" bifurcation to two different WNT states (Figure S9) depending on the choice of just 3 parameters: m, θ_E, and k.

$$\frac{1}{W}=\frac{k}{v_W}*\frac{\theta_E^m}{\theta_E^m+W^m}+1 \qquad (5)$$

More interestingly, it can be shown that, depending on initial conditions or boundary conditions, this system can admit traveling wave solutions that switch from the higher equilibrium state to the lower equilibrium state[7,8]. In 1D these waves travel with a unique shape and have a speed largely dependent on the coupling constant (here D_E) and time scale of E-CAD synthesis and degradation (v_E). Since in our case we have the boundary condition $E(R,t)=0$, then we can have the situation whereby WNT stimulation directs the periphery cells to a WNT "high" equilibrium state that is more stable than the WNT "low" equilibrium state that their more central neighbours are in. This creates an unstable boundary that can only be resolved by a travelling wave solution. By adjusting $m, \theta_E, k, v_E$and D_E ,we can moderate the speed and shape of the wave to fit the profile of WNT responsive cells in the DKK1$^{-/-}$ micropatterns at 12 hours (LEF1) and 48 hours (BRA and SOX17, as measured in Figure 6). As for the previous fit, this parameter space is sufficiently small enough that we can perform a grid search to find the global optima.

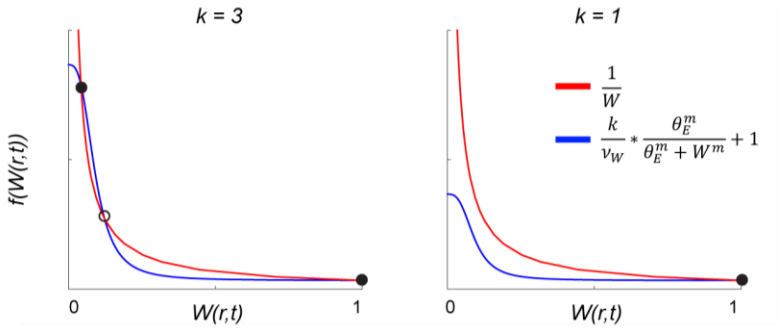

Figure S10: Examples of the cusp bifurcation in Equation 5 with different values of *k*. Solid circles mark stable points, open circles mark unstable points.

The best fit is shown in Figure S11. As for the DKK1 fit, the Hill parameter m can adjust the slope of the curve ($m=3$ in our fit), and to learn the effect of the other parameters we again use selected perturbations. As one might expect, increasing the coupling constant D_E increases the speed of the WNT response wave while decreasing it slows it down. This parameter has the largest effect on wave speed, though changing v_E , the effective turnover rate of E-CAD, also can modify speed since increasing it makes cells next in line in the wave respond faster once the wave reaches them. This can be noted in the perturbation analysis, as changing either D_E or v_E leads to a change in the other

variable to compensate for it. As one expects from Equation 5, θ_E and k are linked, so perturbing one leads to a correction from the other. Due to the non-linearity of the bifurcation they control they are also quite sensitive to perturbation, so just halving or doubling one leads to a collapse of the wave and one dominant state (i.e. either E-CAD is too strong and cells resist the WNT signal, or E-CAD is too weak and even a small WNT signal can downregulate it anywhere).

Perturbing the DKK1$^{-/-}$ fit

	D_E ($mm^2 h^{-1}$)	v_E (h^{-1})	θ_E	k
(1)	0.0043	8.0402	0.09005	2.4184
(2)	0.0086	8.0402	0.09005	2.4184
(3)	0.0086	30.0788	0.0272	9.0474
(4)	0.0021	8.0402	0.09005	2.4184
(5)	0.0021	67.0019	0.0367	6.0619
(6)	0.0043	8	0.09005	2.4184
(7)	0.0058	8	0.0272	9.0474
(8)	0.0043	4	0.09005	2.4184
(9)	0.0058	4	0.1650	1.2217
(10)	0.0043	8.0402	0.1801	20.1534
(11)	0.0332	6.0619	0.1801	1.2217
(12)	0.0043	8.0402	0.0450	20.1534
(13)	0.0045	0.0149	0.0450	6.0619
(14)	0.0043	8.0402	0.09005	4.8368
(15)	0.0548	100	0.0496	4.8368
(16)	0.0043	8.0402	0.09005	1.2092
(17)	0.0905	100	0.1650	1.2092

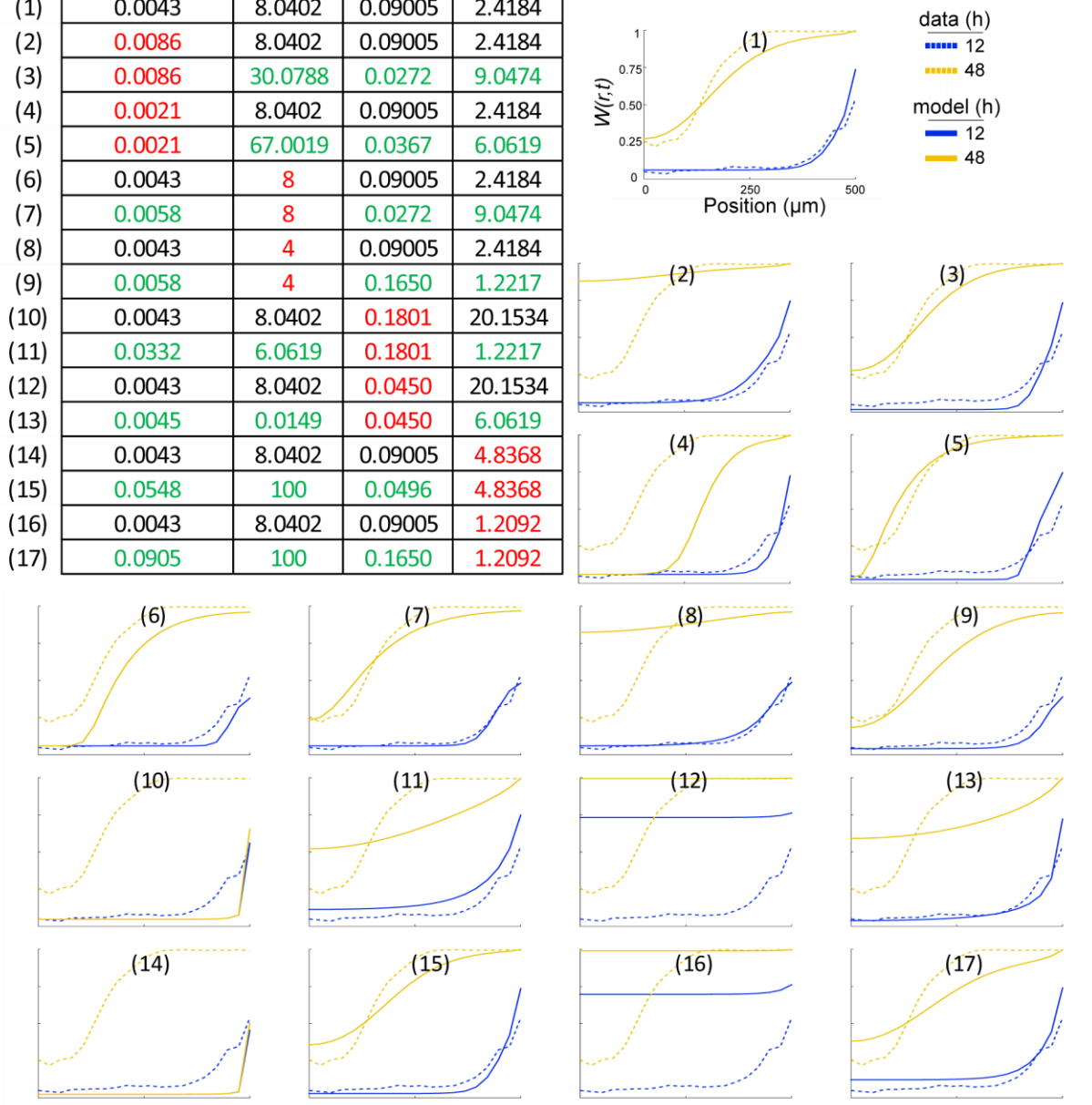

Figure S11: Fit of E-CAD specific parameters with DKK1$^{-/-}$ cell line, and parameter analysis using specific perturbations. Values in black in the table are the best fit parameters, values in red are the parameters specifically perturbed, and values in green are the new best fit parameters based on the perturbed parameter.

2.3 Applying fit to GLR:DKK1$^{-/-}$ time-lapse movie

As discussed in the main text, a further test of our fitted model was to apply it to our live-cell time-lapse GLR:DKK1$^{-/-}$ data. We found that though the model matches the data for the first 30 hours, beyond this there is a collapse of the inner SOX2 region that is quicker than what the model predicts (Figure S12). The agreement is a little better in a repeat of the experiment (Figure S12) but there is still a greater error between the model and these live cell data sets than the fixed antibody stained data we fit to. However the virtual disappearance of the SOX2 domain in the colony center at 72hrs is confirmed by the fixed data in Figure 6, which was not used in the fit. The difficulties in reproducing the movie data could entail the different dynamics of the live fluorescent reporter versus the LEF1 and the SOX2 stain, phototoxicity, or uncontrollable density differences.

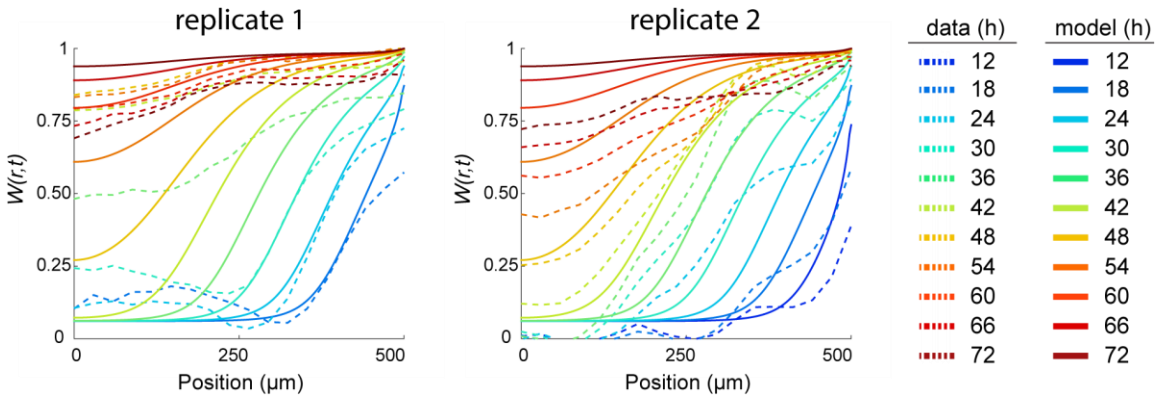

Figure S12: Comparison of the previously fitted model to two replicates of continuously imaged GLR:DKK1$^{-/-}$ micropatterns, the first replicate is an average of 7 colonies, the second replicate is an average of 10 colonies.

3 Mesoderm versus endoderm fate bifurcation

Having obtained the radial profile of differentiated cells from Eqs 1-3 for each cell line, the next question is whether these cells will commit to mesoderm (BRA) or endoderm (SOX17). In the anterior mouse primitive streak, these are two mutually exclusive states that are influenced mainly by the relative levels of WNT versus NODAL signalling, with more WNT signalling leading to mesoderm and more NODAL signalling leading to endoderm. The effect of NODAL signalling on endoderm fate choice was also shown in hESC micropatterns[9] in and reproduced in Fig 1A. Here we do not attempt to model the mechanism for this bistability or capture the dynamics. Instead, we simply let the choice depend on the ratio of WNT to NODAL signalling, letting the differentiated cells go to endoderm with probability $P(r)$ and going to mesoderm with probability $Q(r) = 1 - P(r)$. Since we are focused only on the fraction of cells at each radial position that differentiated, and in our model a differentiated cell is a cell that responded to the WNT signal, we assume that the WNT level is approximately the same across differentiated cells and thus a constant. NODAL signalling however is not the same for all cells, so we use measured nuclear SMAD2 levels for each cell line to approximate it (Figure 5 and Figure S13). Note

that we examine the SMAD2 levels at 24hrs rather than 48hrs, as 48hrs is too late and the fate decision has already been made. Thus our probabilities are

$$P(r) = \frac{NODAL(r)}{WNT(r) + NODAL(r)} = \frac{SMAD2_i(r) - b_1}{b_2 + (SMAD2_i(r) - b_1)} \quad (6)$$

$$Q(r) = \frac{WNT(r)}{WNT(r) + NODAL(r)} = 1 - P(r) \quad (7)$$

This effectively amounts to just a rescaled version of the measured SMAD2 profiles for each of our cell lines.

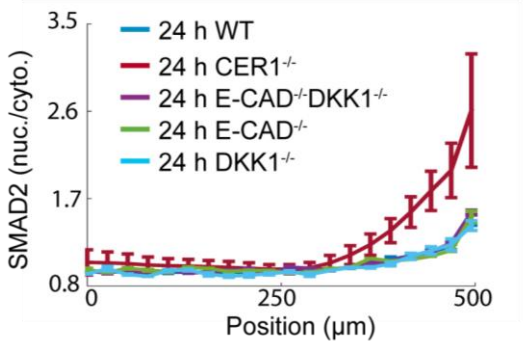

Figure S13: Radial profiles of nuclear SMAD2 in the cell lines modelled, n=20 colonies per condition.

4 Comparison of full model with data

Putting together the PDE system and the fate bifurcation parts of the model and comparing it to the measured SOX2, BRA, and SOX17 radial profiles at 48hrs for each cell line, we see that our model captures the data very well (Figure 7E). One obvious missing feature, however, is the dual SOX17 and BRA positive cell population. These are cells that express both markers and have not yet committed to one fate versus the other (though we expect they will as time progresses) and are found in most significant numbers in the DKK1$^{-/-}$ and E-CAD$^{-/-}$DKK1$^{-/-}$ cell lines. If forced to apportion this population to either mesoderm or endoderm, one can see that classifying them as mesoderm would give the better fit to the model. Interestingly the major exception to this is at the colony edges in the double knockout E-CAD$^{-/-}$DKK1$^{-/-}$ cell line, where doing so would lead the model to underestimate the number of BRA cells counted in the imaging. To further investigate this large discrepancy between the model and the data, we re-examined our E-CAD$^{-/-}$DKK1$^{-/-}$ micropattern data. We found that on the colony edge (and only on the colony edge) BRA cells sometimes lumped together in discrete clusters (Figure S14). As these clusters were immediately surrounded by a monolayer primarily composed of SOX17 cells, instead of the salt-and-pepper BRA or SOX17 pattern found further in the interior of the colony, we suppose that these clusters formed due to cell movement, i.e. cells were initially patterned in a stochastic manner but the BRA cells then moved and coalesced together while the SOX17 cells either stayed in place or underwent unbiased migration. That this only takes place on the edge of the E-CAD$^{-/-}$DKK1$^{-/-}$ micropatterns could be explained by noting that it is in this regime that cells are the least restricted from

moving, both by E-CAD and by existence of neighbours. The clusters are often quite 3 dimensional, and since our analysis involves just 2D segmentation on epifluorescence images, classification of cells in these clusters may be biased and introduce errors such as overcounting the number of SOX17/BRA cells. Migration was also not included in the model, and introducing a biased outward migration term for BRA cells for example might lead to an improved (though more complex) fit.

Overall, our model faithfully captures the E-CAD and DKK1 patterning dynamics as observed in our micropatterns and live-reporter lines, and in the most striking case where it does not, it still proves informative, pointing to a segregation and clustering of mesoderm versus endoderm cells that may be due to cell migration and merits further investigation.

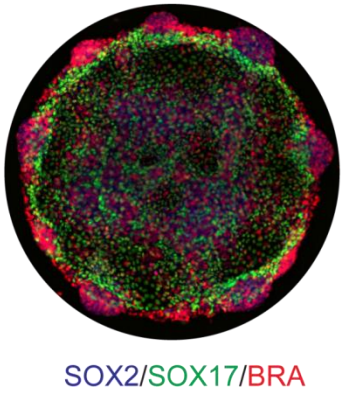

Figure S14: Example of an E-CAD$^{-/-}$DKK1$^{-/-}$ micropattern with BRA clusters on the periphery. The center remains a salt-and-pepper mix of SOX17 and BRA cells.

1. Etoc, F. *et al.* A Balance between Secreted Inhibitors and Edge Sensing Controls Gastruloid Self-Organization. *Dev. Cell* **39,** 302–315 (2016).

2. Libusova, L., Stemmler, M. P., Hierholzer, A., Schwarz, H. & Kemler, R. N-cadherin can structurally substitute for E-cadherin during intestinal development but leads to polyp formation. *Development* **137,** 2297–2305 (2010).

3. Cruciat, C. M. & Niehrs, C. Secreted and Transmembrane Wnt Inhibitors and Activators. *Cold Spring Harb. Perspect. Biol.* **5,** 39–64 (2013).

4. Arnold, S. J. & Robertson, E. J. Making a commitment: cell lineage allocation and axis patterning in the early mouse embryo. *Nat. Rev. Mol. Cell Biol.* **10,** 91–103 (2009).

5. Fagotto, F. Looking beyond the Wnt pathway for the deep nature of β-catenin. *EMBO Rep.* **14,** 422–33 (2013).

6. Kam, Y. & Quaranta, V. Cadherin-bound β-catenin feeds into the Wnt pathway upon adherens junctions dissociation: Evidence for an intersection between β-catenin pools. *PLoS One* **4,** (2009).

7. Fisher, R. A. The Wave of Advance of Advantageous Genes. *Ann. Eugen.* **7,** 355–369 (1937).

8. Tikhomirov, V. M. in *Selected Works of A. N. Kolmogorov: Volume I: Mathematics and Mechanics* (ed. Tikhomirov, V. M.) 242–270 (Springer Netherlands, 1991). doi:10.1007/978-94-011-3030-

1_38

9. Martyn, I., Kanno, T. Y., Ruzo, A., Siggia, E. D. & Brivanlou, A. H. Self-organization of a human organizer by combined Wnt and Nodal signalling. *Nature* **558,** 132–135 (2018).